J Mater Sci (2016) 51:10229–10244

The impact of liquid crystal fillers on structure and properties of liquid-crystalline shape-memory polyurethane composites I: 4-dodecyloxybenzoic acid

Jianfeng Ban[1,2], Linjiang Zhu[1], Shaojun Chen[1,*], and Yiping Wang[2,*]

[1] *Shenzhen Key Laboratory of Polymer Science and Technology, Shenzhen Key Laboratory of Special Functional Materials, Nanshan District Key Lab for Biopolymers and Safety Evaluation, Guangdong Research Center for Interfacial Engineering of Functional Materials, College of Materials Science and Engineering, Shenzhen University, Shenzhen 518060, China*

[2] *Key Laboratory of Optoelectronic Devices and Systems of Ministry of Education and Guangdong Province, College of Optoelectronic Engineering, Shenzhen University, Shenzhen 518060, China*

Received: 15 June 2016
Accepted: 21 July 2016

ABSTRACT

Aiming to elucidate the influence of liquid crystal fillers on the structure and properties of liquid-crystalline (LC) shape-memory polyurethane (SMPU) composites, a series of LC-SMPU composites are successfully prepared by adding various concentrations of 4-dodecyloxybenzoic acid (DOBA) to shape-memory polyurethane containing 40 wt% hard segment content (SMPU40). The structure, morphology, thermal properties, liquid crystalline properties, and shape memory properties are systematically investigated. The results demonstrate that DOBA is successfully incorporated into the polymer matrix of SMPU40 without interrupting the dimerization structure of DOBA that allows it to exhibit LC properties. The incorporated DOBA not only improves the crystallizability of the soft segment but also promotes the crystallizability of the hard segment. The isothermal crystallization kinetics further reveal that the crystallization rate of the hard segment decreases as the DOBA content increases, and the crystallization of the LC-SMPU composites nucleates in a similar manner. The LC-SMPU composites are composed of a DOBA phase and an SMPU phase, which further forms soft phase–hard phase microphase separation structures. The composite tends to only maintain the nematic LC properties of DOBA due to the interruption of polyurethane chains. However, the LC-SMPU composites exhibit good triple-shape memory effects. The first step of strain recovery is associated with the melting transition of soft segment crystals of the polyurethane matrix, and the second step of strain recovery is resulted from the melting transition of the DOBA crystals.

Address correspondence to E-mail: chensj@szu.edu.cn; ypwang@szu.edu.cn

DOI 10.1007/s10853-016-0251-7

Introduction

Shape-memory polymers (SMPs) are a promising class of responsive polymeric materials with the ability to be programmed to take temporary shape and then recover to their permanent shape when exposed to an external stimulus [1–5]. Compared to shape-memory alloys (SMAs), the advantages of SMPs include high shape deformability, light weight, large recovery ability, lower cost, and superior process ability [6, 7]. Shape memory is usually a thermally induced process. The shape memory effect (SME) of thermally activated SMPs requires the combination of a reversible thermal transition and a mechanism for setting the permanent shape. The former is referred to as a shape memory transition and is commonly a crystal melting or glass transition, whereas the latter can be physical or chemical crosslinking. A variety of thermal SMPs have been reported with a wide range of activation temperatures and applications, such as use in medical devices, heat shrinkable packages for electronics, mechanical actuators, sensors, high-performance water–vapor permeability materials, and self-deployable structures [8–10].

Among thermal SMPs, shape-memory polyurethane (SMPU) has most often been used in practice due to its competitive mechanical and shape memory properties [11, 12]. However, the most common SMPU that exhibits SMEs has not met the growing trend of new multifunctional materials. Recently, shape-memory polymer composites (SMPCs) have gained significant interest due to their convenient and efficient actuation methods [1, 13] using multimaterial approaches, and new functions, such as unique electrical, magnetic properties, and radio-opacity and biofunctionality, can be added to SMPs by incorporating small amounts of active fillers into the polymer matrix. SMPCs can be doped with conductive fillers. Then SMPCs can be actuated through Joule heat by simply passing an electric current through the SMPCs, instead of using external heaters, inconvenient devices, or a bulk system to generate the actuating environment [14, 15]. Similarly, SMPCs containing a small amount of magnetic particles, such as iron oxide or nickel zinc ferrite, can be inductively actuated by applying an alternating magnetic field [16, 17]. In addition, the incorporation of high-modulus inorganic or organic fillers into SMP matrices leads to improved mechanical strengths and shape recovery stress. Investigations of SMPCs have indicated a promising research direction in the field of SMPs and polymer composites. Thus, SMPCs represent a new way to prepare polymer composites with diversified shape memory properties.

Liquid-crystalline (LC) materials are one type of functional filler that has been widely used to fabricate LC polymer composites and has recently attracted much attention [18–21]. Finkelmann and coworkers reported a shape-memory LC elastomer, which can be stimulated via photo-illumination by incorporating azo groups into the LC mesogens [22]. Upon UV radiation, the azo groups isomerize from the *trans* to the *cis* configuration and sharply bend the mesogens, hindering the nematic ordering. Samit et al. synthesized a new triblock copolymer with a large central block composed of the main-chain nematic polymer that retains the director alignment and exhibits a marked SME [23]. The microphase separation driven by the nematic transition in the midblock is fast and reliably reproducible after reheating. The shape memory response of the nematic elastomer is due to the highly anisotropic conformation, with the chain folded into hairpins. Previous studies on SMPs with LC properties have primarily focused on LC elastomers or polymers for double-SMEs or triple-SMEs. In addition, some LC shape-memory polyurethane composites (LC-SMPCs) have been reported. Both the semicrystalline of the soft phase of the SMPU matrix and the LC phase can be used to trigger SMEs.

In our previous studies, we developed a facile and versatile method for the preparation of LC-SMPCs, which not only maintained the LC properties in the polymer but also induced a multi-SME. We have systematically researched the multishape memory properties and tunable LC properties of composites based on various SMPU matrices and 4-*n*-hexadecyloxybenzoic acid (HOBA) fillers [24, 25]. Our previous investigations also demonstrated that LC-SMPCs filled with 4-*n*-octyldecyloxybenzoic acid (OOBA) have good multi-SMEs, exhibiting triple-SMEs and quadruple-SMEs [26]. Therefore, we proposed that LC-SMPCs are good candidates for many potentially applications in smart optical devices, smart electronic devices, and smart sensors. It is well known that 4-dodecyloxybenzoic acid (DOBA) is a liquid-crystalline material that exhibits both a nematic LC phase and a smectic LC phase upon heating [27, 28]. However, there are no reports of SMPCs with fillers of DOBA mesogens. The significant effects of mesogens on the glass transition and crystal melting of the soft phase have been reported for HOBA-SMPU and OOBA-SMPU systems. However, the influence on the hard phase or hard domains is still unclear.

In this work, we developed another series of LC-SMPCs with both LC properties and shape memory properties. In contrast to the previous systems, a SMPU containing approximately 40 wt% hard segment was selected for the polymer matrix in this experiment, because a semicrystalline soft phase and an amorphous hard phase were formed in this SMPU40. To achieve both a nematic LC phase and a smectic LC phase in the LC-SMPCs, DOBA mesogens were added to the SMPU40 polymer matrix. Our preliminary results show that the DOBA filler markedly promoted crystallization of the hard phase. The thermal properties, LC properties, and shape memory properties of the SMPU40/DOBAm systems were quite different from previous systems. This study lays the foundation for the multifunctional properties, multiple responses, and efficient actuation of this type of composite.

Experimental section

Materials

Extra pure-grade polyethylene glycol ($M_n = 6000$, PEG6000) was dried beforehand at 80 °C under 0.1–0.2 MPa for 6 h. 4,4-Diphenylmethane diisocyanate (MDI, analytical grade), 1,4-butanediol (BDO, analytical grade), 4-dodecyloxybenzoic acid (DOBA, analytical grade), and dimethylformamide (DMF, high-performance liquid chromatography grade, solvent) were purchased from Aladdin Chemical Reagent Co. Ltd. (Shanghai, China) and were used without further purification.

Synthesis of shape-memory polyurethane

According to our previous study [13], the PEG-based SMPU with 40 wt% hard segment content, termed SMPU40, was easily synthesized via a bulk polymerization method using MDI, BDO, and PEG6000. The synthesis route is presented in Scheme 1. The polymerization procedures were as follows: 30.00 g of PEG and 15.53 g of MDI were added to a 500-mL conical flask equipped with a mechanical stirrer, and the prepolymer was constantly stirred at 60 °C for 20 min. Next, 4.47 g of BDO was added to the reaction for another 10 min for chain extension. Subsequently, the resulting prepolymer was poured into a Teflon pan for a post-curing process at 80 °C under a vacuum for 10 h, and the target SMPU40 resin was obtained.

Preparation of the LC-SMPU composites

A 10 wt% SMPU40/DMF solution was first prepared by dissolving the obtained bulk SMPU40 resin in DMF at 80 °C for 48 h. According to the composition of the composites, as illustrated in Table 1, the samples were coded as P1-P4 (SMPU40/DOBAm, $m = 0.2, 0.4, 0.6, 0.8$, which is the molar ratio of C=O/N–H). Taking P1 (SMPU40/DOBA0.2) as an example, 0.2 g of DOBA was added to the SMPU40/DMF solution containing approximately 3.0 g SMPU40 resin. After strong mechanical stirring at 80 °C for 2 h, SMPU40 and DOBA were fully mixed to obtain a homogeneous solution-phase mixture. Finally, the P1 composite for the following tests was obtained by casting the mixture in a Teflon pan, which was placed at 80 °C for 24 h and further dried at 80 °C under a vacuum of 0.1–0.2 MPa for 24 h.

Instruments and measurements

FT-IR spectra were scanned from smooth 0.2-mm-thick polymer films using a Nicolet 6700 FT-IR spectrometer by according to the FT-IR attenuated total reflection (ATR) method. Ten scans at a resolution of 4 cm^{-1} were signal averaged and stored—for further analysis.

XRD experiments were performed using a BRUKER AXS D8 Advance diffractometer with a 40 kV FL tube as the X-ray source (Cu Kα) and a LYNXEYE-XE detector.

DSC testing was performed using a TA Q200 instrument with nitrogen as the purged gas. Indium and zinc standards were used for calibration. Samples were first heated from −60 to 150 °C at a heating rate of 10 °C/min and kept at 150 °C for 1 min, subsequently, cooled to −60 °C at a cooling rate of 10 °C/min, and finally heated a second time from −60 to 150 °C.

After drying at 100 °C, TGA curves were recorded on a computer-controlled TA Instrument TG Q50 system, under the following operational conditions: a

Scheme 1 Synthesis route of SMPU40.

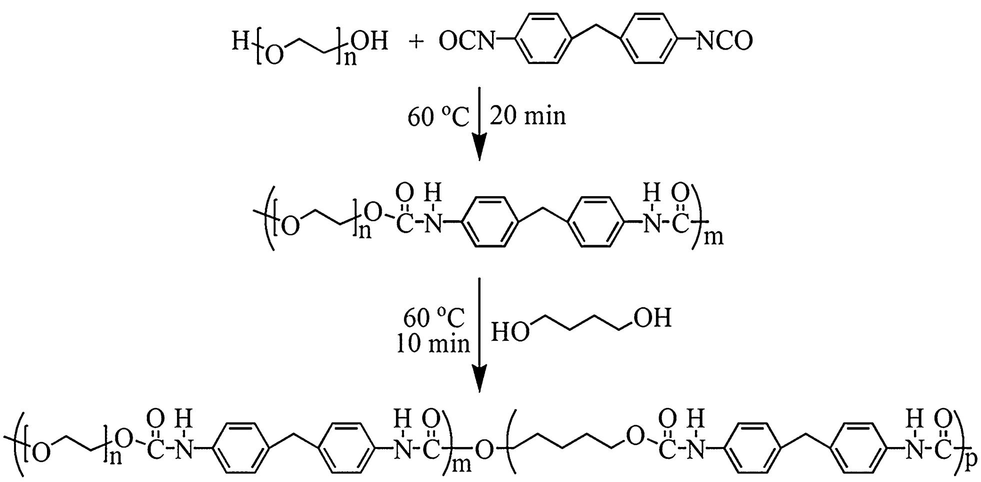

Table 1 Composition of the SMPU40/DOBAm composites

Samples	SMPU40 (g)	DOBA (g)	Molar ratio of C=O/N–H
SMPU40	3	–	–
P1 (SMPU40/DOBA0.2)	3	0.200	0.2
P2 (SMPU40/DOBA0.4)	3	0.399	0.4
P3 (SMPU40/DOBA0.6)	3	0.598	0.6
P4 (SMPU40/DOBA0.8)	3	0.797	0.8

heating rate of 10 °C/min, a temperature range of 100–600 °C, a sample weight of approximately 5.0 mg, using film specimen in platinum crucibles, and 60 mL/min N_2 flow. Three or four repeated readings (temperature and weight loss) were made for the same TG curve, each including at least 15 points.

A POM microscope (Mshot, China) equipped with a hot stage (Mettler Toledo FP90 Central Processor & FP82 Hot Stage) and a camera were used to observe and record the strain recovery behaviors of the sample upon heating and cooling at a rate of 2 K/min.

A Nanonavi E-Sweep (SII Nanotechnology Inc.) atomic force microscope (AFM) was used in tapping mode for the morphological characterization of the dried sample. The samples were dissolved in DMF at a concentration of 5 mg/mL and first spin coated at 400 rpm for 10 s followed by 4000 rpm for 60 s on oxidized silicon substrates. Spin-coated films were kept in a 50 °C oven for 48 h to evaporate the solvent.

DMA curves of the samples were determined using a TA DMA800 system at 1 Hz and at a heating rate of 2 °C/min. The change in the modulus and the recovery stress were measured using the DMS module and TMA module, respectively.

Characterization for isothermal crystallization kinetics

Isothermal crystallization experiments were performed using a TA Q200 DSC instrument with nitrogen as the purge gas. The sample (4–6 mg) was initially heated to 230 °C at a rate of 10 °C/min and held for 5 min to remove the thermal history of the crystallizable phase. Subsequently, the sample was rapidly cooled (−60 °C/min) to a designated crystallization temperature (T_c) and held at this temperature until the end of the exothermic crystallization. The heat flow during the isothermal crystallization process was recorded as a function of time. T_c was chosen as 137 °C in this experiment. The amounts of heat generated during the development of the crystal phase were recorded and analyzed according to the typical equation used for evaluating the degree of relative crystallinity (X_t):

$$X_t = \frac{\int_{t_0}^{t}\left(\frac{dH}{dt}\right)dt}{\int_{t_0}^{t=\infty}\left(\frac{dH}{dt}\right)dt}, \tag{1}$$

where t_0 and $t = \infty$ are the times at which the sample reached isothermal conditions (as indicated by a flat baseline after an initial spike in the thermal curve) and the time at which the dominant sharp exothermic peak ended, respectively. H is the enthalpy of crystallization at time t. After isothermal crystallization, the sample was heated to 100 °C, and the T_m, indicated by the maximum of the endothermic peak, was recorded.

The crystallization kinetics were analyzed according to the modified Avrami equation, known as the Ozawa equation:

$$X(t) = 1 - \exp(-Kt^n). \qquad (2)$$

Equation (2) can be converted into the following form:

$$\log\{-\ln[1 - X(t)]\} = n \log t + \log K. \qquad (3)$$

A plot of $\log\{-\ln[1-X(t)]\}$ against $\log t$ should yield a straight line. By fitting the lines, n and $\log K$ can be calculated from the slope and intercept, respectively.

Additionally, the half-crystallization time [$t(0.5)$] is defined as the time at which the crystallinity is equal to 50 % and is related to the Avrami parameter K as determined by the following expression:

$$K = \ln 2/[t(0.5)]^n. \qquad (4)$$

Results and discussion

Structural analysis

Figure 1 shows the FT-IR spectra of the SMPU40/DOBAm composites, SMPU40 and DOBA. As shown in Fig. 1a, a C=O stretching vibration was detected at approximately 1687 cm^{-1} in the spectrum of DOBA, which indicated that the dimerization through hydrogen bonding creates a long lath-like structure with a three-ring core in the composite, retaining the basic structure of DOBA to form the liquid crystal. Compared with SMPU40 [29], the LC-SMPU composites, e.g., P4 (SMPU40/DOBA0.8), showed new frequencies at approximately 1360, 975, and 910 cm^{-1}. These new frequencies were also observed in the DOBA spectrum, which confirmed that the DOBA was successfully incorporated into the SMPU40 to form composites. In addition, N–H stretching vibrations showing the formation of urethane groups of SMPU40 and P4 were observed at 3323 and 3311 cm^{-1}, and no –N=C=O characteristic absorption peak was observed at approximately 2260 cm^{-1}. Thus, isocyanate had reacted completely. However, no significant variations were found in the N–H vibration frequency at approximately 3396 cm^{-1} or the C=O vibration frequency at 1669 cm^{-1} among the SMPU40/DOBAm composites (as shown in Fig. 1b). These results imply that the doped DOBA did not influence the hydrogen bonding between the N–H group and the C=O group of the urethane groups. Additionally, the absorption frequency of N–H was shifted to a lower wave number when DOBA was incorporated into the SMPU40. Since DOBA combined with the hard segment, the composites likely formed stabilized hard segment aggregations or hard segment crystallizations. In the previous report, the LC mesophase was lost when the LC mesogens containing pyridine moieties were attached to the SMPU containing

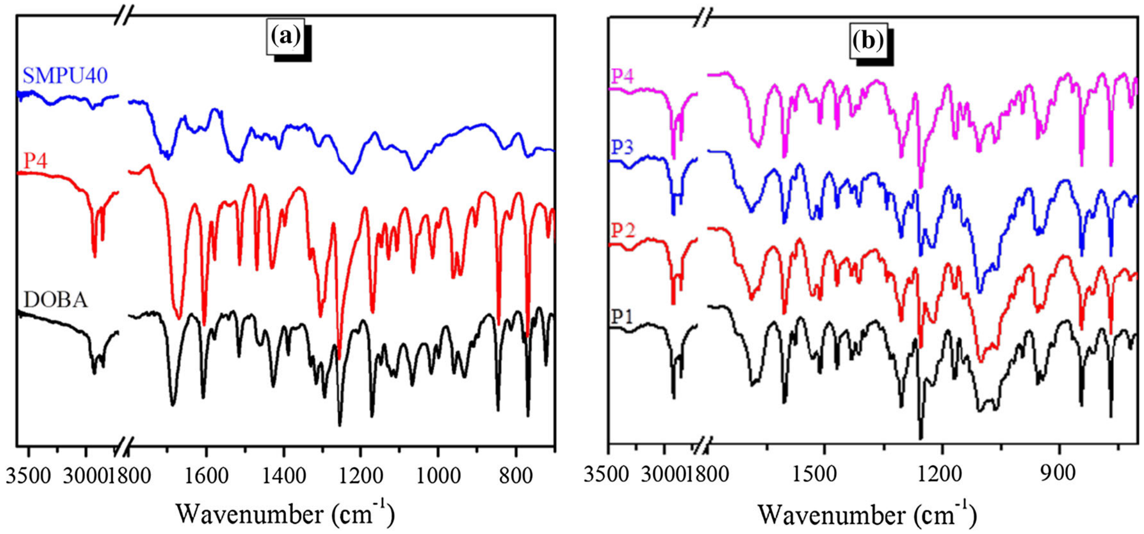

Fig. 1 FT-IR spectra of **a** P4 compared with SMPU40 and DOBA, **b** SMPU40/DOBAm.

carboxyl groups, which were attached through hydrogen bonding between pyridine and COOH [30]. However, the present SMPU40/DOBAm composites maintained the intrinsic LC properties of DOBA. Compared with DOBA, the first advantage of SMPU40/DOBAm composites is that the LC properties of DOBA can be used in the form of a polymer for many applications.

Morphology analysis

The surface morphology of the SMPU40/DOBAm composite film was investigated systematically via SEM and AFM. Figure 2 shows the SEM images of the SMPU40/DOBAm composites with various DOBA contents. As shown in Fig. 2, SMPU40 exhibited a smooth surface without any holes. When DOBA was doped into the SMPU40, as shown in Fig. 2a–d, cracks appeared on the surfaces of the samples as the DOBA content increased. Therefore, a high fraction of DOBA filler may destroy the form of the polymer film, whereas a suitable level of doping with DOBA filler could endow the SMPU40/DOBAm composite film with LC properties of DOBA. Additionally, the SEM images in Fig. 2c, d revealed the two-phase separated structure composed of the crystalline DOBA phase and the amorphous polyurethane matrix. Several self-assembled crystals were

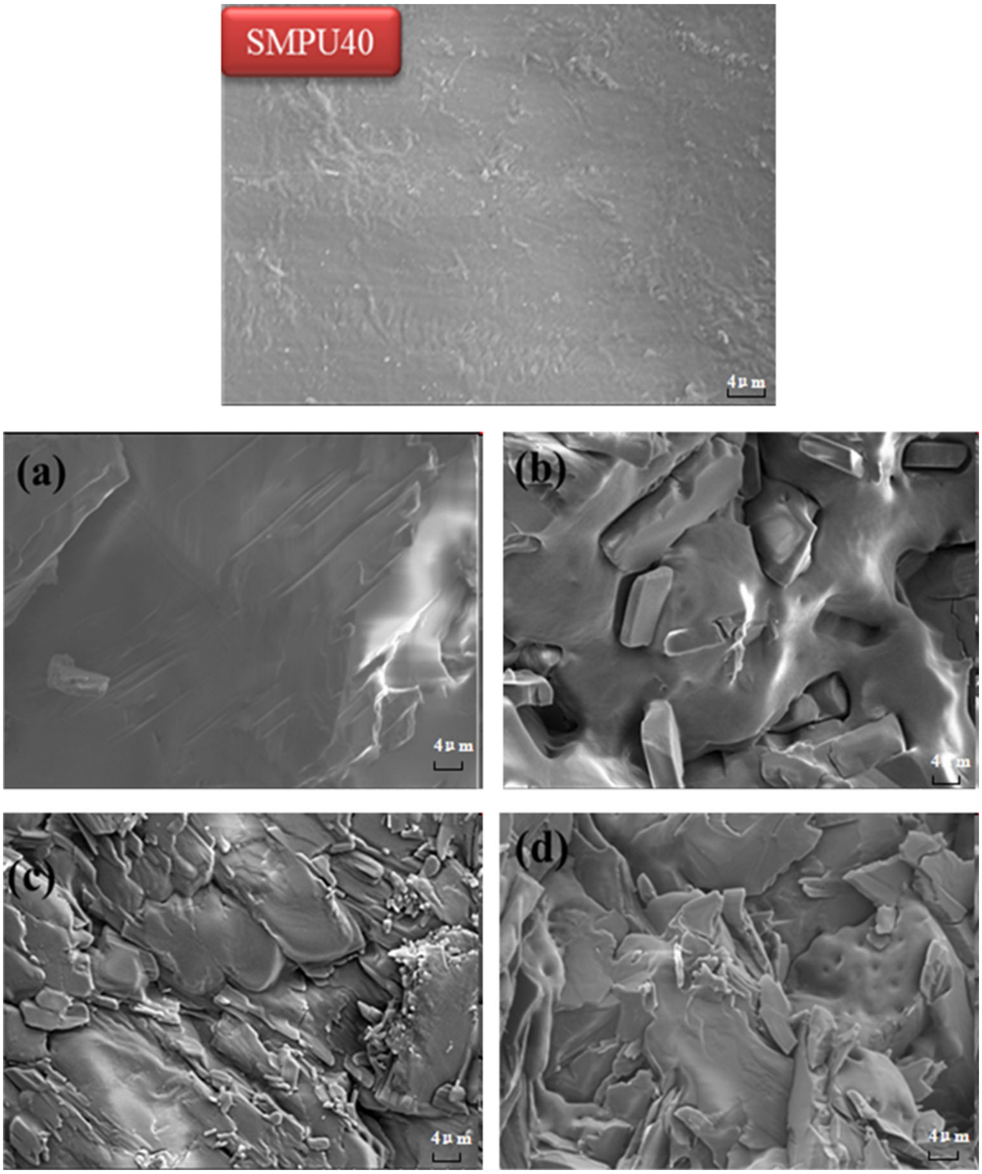

Fig. 2 SEM images of SMPU40, **a** P1, **b** P2, **c** P3, and **d** P4, respectively.

observed in the magnified SEM image of the samples P3 and P4. Taking P4 as an example, these self-assembled crystals were likely formed by the free DOBA crystals, whereas the other DOBA molecules could not be precisely estimated because they were wrapped into a very small size by the polyurethane matrix. Thus, the doped DOBA not only entered the polyurethane matrix but also self-assembled into the free DOBA phase in the composites. Both the wrapped DOBA phase and the free DOBA phase still exhibited liquid crystalline properties upon heating and cooling, because DOBA dimerization was maintained, as discussed in the structure analysis; the same results will be discussed for the POM analysis. Based on the SEM results, we confirmed that the SMPU40/DOBAm composites were composed of separate structures: a crystalline DOBA phase and a polyurethane matrix.

A typical AFM image further confirmed the formation of a microphase structure composed of a hard phase and a soft phase in the polyurethane matrix. The AFM image corresponds to a 1ìm, selection from the polyurethane matrix. As can be seen in Fig. 3, the height and phase 3D images show that light and shaded cross-distribution microareas exist in the polyurethane matrix, and outshoots appear throughout the surface, which correspond to the light colored parts in the AFM images and may be aggregated hard segments of polyurethane serving as the hard phase [31]. The concave parts, which present continuous phases, may be aggregation of the soft phase [31, 32]. The continuous repeating peak indicates that the polyurethane matrix maintained good microphase separation between soft segment and hard segment, the doped DOBA also promoted the formation of soft and hard segment microareas, which were identified in the DSC and DMA results. This microphase separation structure provides a morphology foundation that exhibits shape memory properties.

To further study the structure and morphology of the SMPU40/DOBAm composites, an XRD experiment was conducted. The XRD results showed that all the samples were crystalline and exhibited various degrees of crystallinity. As shown in Fig. 4, the XRD pattern of DOBA shows many sharp peaks located in

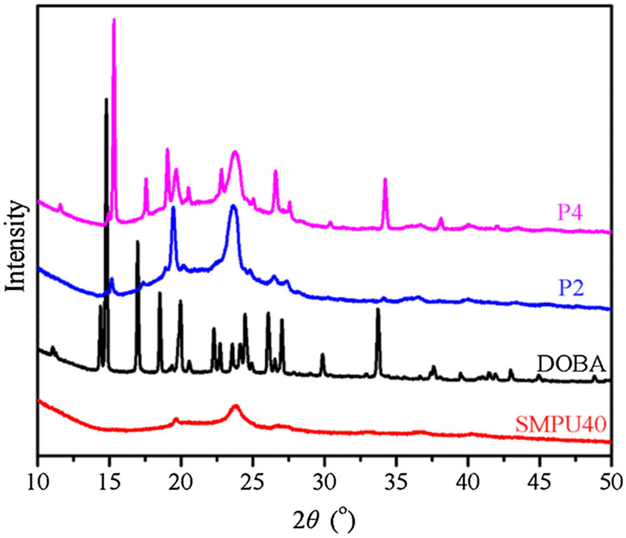

Fig. 4 XRD patterns of SMPU40, DOBA, P2, and P4, respectively.

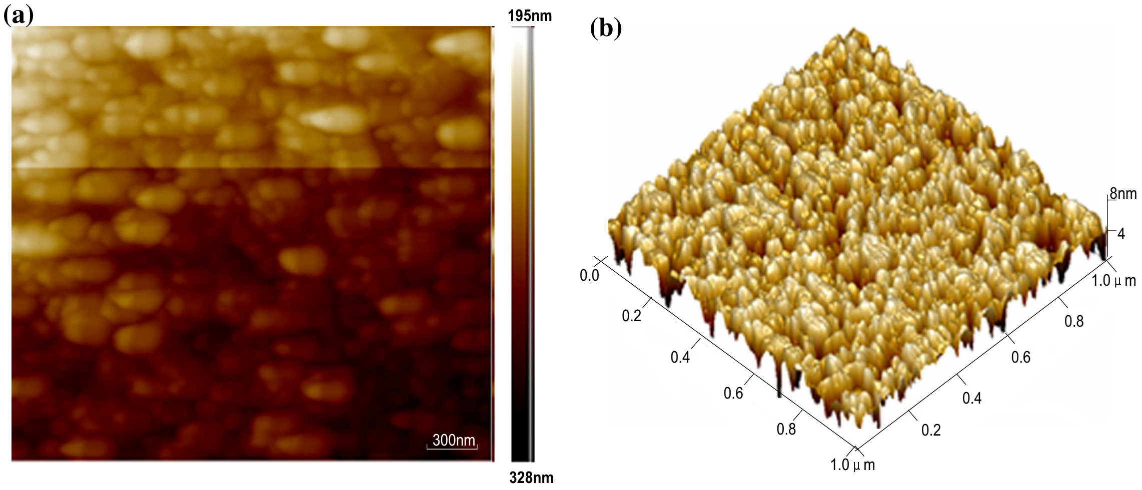

Fig. 3 Typical AFM images (**a** 2D height; **b** 3D phase) of polyurethane matrix in P4.

the wide-angle region at 10°–35°, indicating that DOBA was a complete crystalline material. Due to the weak degree of crystallinity of the soft segment of SMPU40; over the test region of 2θ from 10° to 35°, only three weak and broad peaks were observed in the XRD pattern of SMPU40, located at 19.6°, 23.8°, and 26.9°. With DOBA incorporated into the SMPU40, the intensity of crystallinity increased, indicating that the completely crystalline DOBA can promote the crystallinity of the soft segment of SMPU40. However, a few crystalline peaks corresponding to DOBA disappeared in the SMPU40/DOBAm composites, when the DOBA content was under 0.4 wt%. Comparing P4 with P2, as shown in Fig. 4, the crystallinity of DOBA in P2 was more easily destroyed by SMPU40, and therefore, the crystallinity of DOBA in P2 was not as high as in pure DOBA. For increasing contents of DOBA, the intensity of the crystallinity peak increased because higher contents of DOBA lead to increased DOBA dimerization, which forms the LC structure. Due to the interaction between DOBA and polyurethane, the crystal regularity of DOBA was reduced, and thus, the diffraction peaks of the SMPU40/DOBAm composites broaden and shifted to higher angles compared to DOBA. These influences may also be reflected in the thermal properties and phase transitions.

Thermal properties

The thermal properties of the SMPU40/DOBAm composites were investigated via TGA and DSC. Thermal stability is an important property for applications of polymeric materials. The TG-DTG curves of each sample were analyzed and are shown in Fig. 5. The TG curves show that two decomposition stages appeared in all samples, corresponding to the decomposition of the soft segments and hard segments of the polyurethane, respectively (see Fig. 5a). Additionally, the corresponding decomposition temperatures for the SMPU40/DOBAm composites were higher than for SMPU40, and the quantity of the first decomposition stage increased as the content of DOBA increased. One possible reason is that DOBA promotes the microphase separation of the polyurethane matrix, as discussed above, which improves the thermal stability. Furthermore, the DTG curves reveal that the maximum decomposition temperatures of the first stage in the composites were also higher for SMPU40 (see Fig. 5b). One explanation for this difference may be that the decomposition degree of the SMPU40/DOBAm composites was restrained when DOBA was doped into the SMPU40.

DSC instruments have been widely used to study the phase transitions of polymers. Figure 6a presents the DSC curves of SMPU40, P3 (SMPU40/DOBA0.6), and DOBA during the second heating cycle. SMPU40 shows an exothermic peak at approximately −7.6 °C and an obvious endothermic peak at approximately 49.5 °C, corresponding to the cold crystallization temperature and the crystal melting temperature of the soft phase [24], respectively. DOBA also has a similar cold crystallization corresponding to an exothermic peak at approximately 28 °C. Moreover, three obvious endothermic peaks appeared at approximately 97, 134, and 145 °C, respectively. In contrast to the phase transition of HOBA and OOBA, these peaks revealed that the DOBA formed one type of crystal, which is consistent with the previous report. First, upon heating to 97 °C, the crystal DOBA began to melt and then converted to a smectic phase. Second, as the temperature increased to 134 °C, DOBA exhibited a phase transition from a smectic phase to nematic phase. Finally, DOBA was converted to the isotropic phase when the temperature exceeded 145 °C. When DOBA was introduced to SMPU40, forming the SMPU40/DOBAm composites, e.g., sample P3, the cold crystallization of the exothermic peaks observed in SMPU40 and DOBA disappeared, as shown in Fig. 6a. Therefore, the crystallization capacity of the soft segment of SMPU40 was enhanced upon DOBA introducing. In addition, the regularity of DOBA was interrupted by the SMPU40 polymer chain, and therefore, the crystallization capacity of DOBA declined. The crystal melting transition of DOBA weakened and the liquid crystalline phase transitions particularly changed in the SMPU40/DOBAm composites. Figure 6b, c further shows the influence of DOBA on the thermal properties of the composites. For the second heating curves, in the composites with lower DOBA content, e.g., P1 and P2, no phase transition for DOBA mesogens was detected. Even for the composites with higher DOBA contents, e.g., P3 and P4, only the crystal melting transition appeared at approximately 95 °C, and no LC phase transitions were detected. Based on these results, the SMPU40 polymer chain may affect the ordered arrangement of the DOBA mesogens. Additionally, the second heating curves

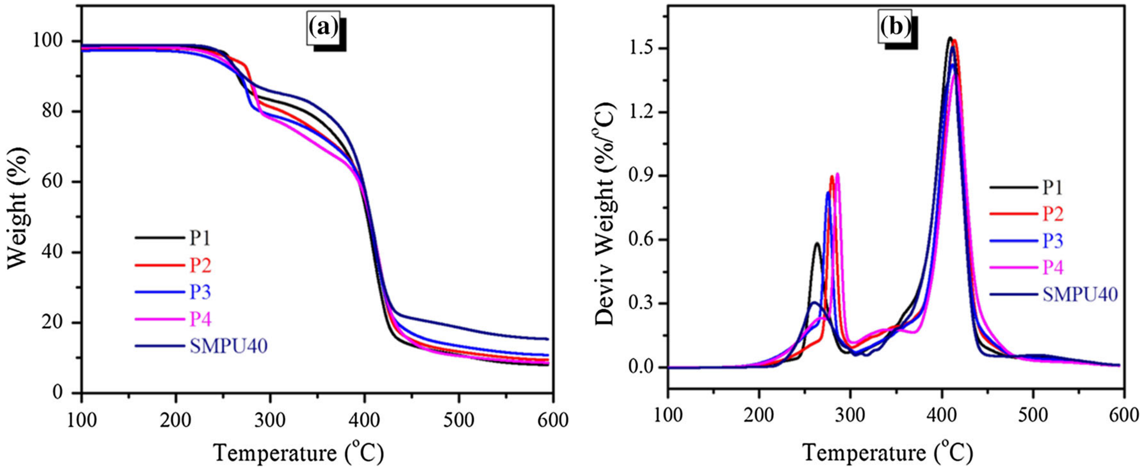

Fig. 5 TG-DTG curves of the samples: **a** TG curves and **b** DTG curves.

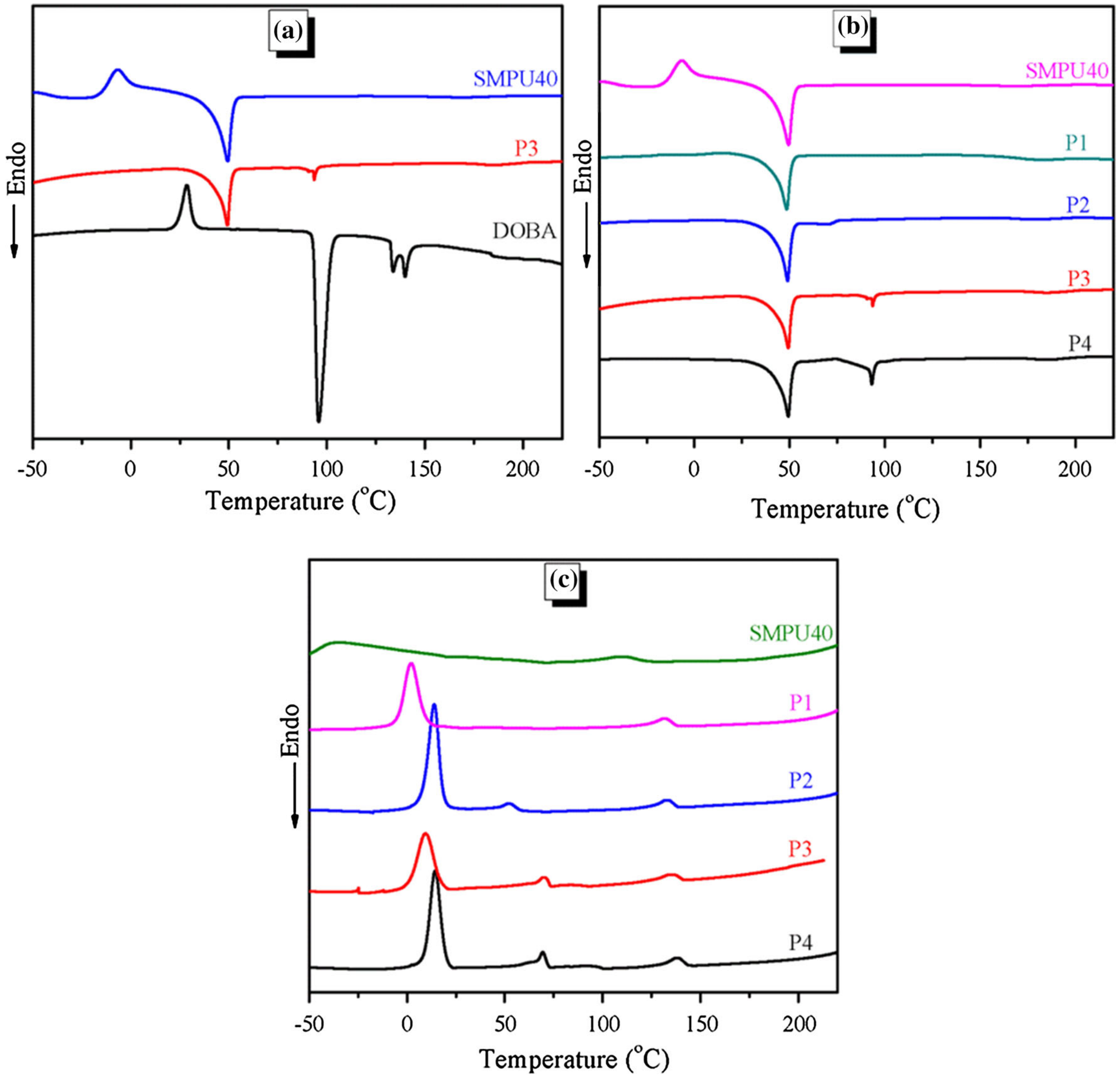

Fig. 6 DSC curves of the samples. **a** The second heating curves of DOBA, SMPU40, and P3. **b** The second heating curves of SMPU40/DOBAm. **c** The first cooling curves of SMPU40/DOBAm.

demonstrate that all composites show no cold crystallization, and the same crystal melting transitions peak was observed at approximately 49.5 °C. This result implies that DOBA promoted the crystallization of the soft phase of polyurethane by serving as only crystal seeds. However, the crystallization capacity of the hard segment of SMPU40 was enhanced upon introducing DOBA. A weak endothermic peak tended to appear above 170 °C on the second heating curve of the composites. Compared to SMPU40, the crystallization temperature of the hard phase became apparent and shifted to higher temperatures at 140 °C on the cooling curves in all the SMPU40/DOBAm composites (see Fig. 6c). The cooling curves also demonstrate that the crystallization temperature of the soft segment of SMPU40 shifted to a higher temperature range. This result further confirms that the crystallinity of the soft segment is promoted by DOBA. Similarly, only one crystallization peak of DOBA was detected on the cooling curve for the composites with high contents of DOBA, which further confirmed that only one type of crystal is formed in the composites. Moreover, the crystalline peak also shifts to higher temperatures from approximately 52 °C in sample P2 to approximately 70 °C in samples P3 and P4. This result again confirms that the doped DOBA is first wrapped by the polyurethane matrix. They further aggregate into an isolated DOBA phase, forming perfect crystallization when the molar ratio of DOBA is higher than 0.4.

To further understand the crystallization behaviors of the SMPU40/DOBAm composites, the isothermal crystallization process was investigated using a DSC instrument. The experimental results are shown in Fig. 7. The detail calculations are provided in "Characterization for isothermal crystallization kinetics". Figure 7a shows that the isothermal crystallization exothermic peak of the SMPU40/DOBAm composites became increasingly wider as the DOBA content increased. This result indicates that the crystallization time increases with increasing DOBA content. According to Eq. 1, the relative crystallinity (X_t) can be calculated. The relationship between X_t and time are shown in Fig. 7b. The result curves exhibit an S pattern, which implies that the rate of crystallization was slow not only during the initial phase but also during a later period of crystallization. Moreover, Fig. 7b shows that the slope of the curves decreased as the content of DOBA increased. This result indicated that the rate of the crystallization declined as the DOBA content increased.

The Avrami equation (Eq. 2) was used to denote the entire crystallization behavior of the SMPU40/DOBAm composites. Generally, for convenient analyses, the Avrami equation is converted to Eq. 3 via linearization. Figure 7c presents the dependency of $\log\{-\ln[1-X(t)]\}$ on $\log t$. Figure 7c demonstrates that $\log\{-\ln[1-X(t)]\}$ and logt have a good linear relation. All the squared values of R were higher than 0.98. According to the original data and the results of fitting a straight line, the isothermal crystallization kinetic parameters of n, K and $t_{1/2}$, were easily calculated, and the results are summarized in Table 2. As observed the results shown in Table 2, the n value of all the samples was ~1.3, indicating that the crystallization of the SMPU40/DOBAm composites nucleated in a similar manner. In addition, the crystallization rate declined, because the K value decreased as the DOBA content increased. Taking the crystallization temperature at 137 °C as an example, on one hand, as the temperature rises to 137 °C, two DOBA molecules create an on-limits binary cyclic structure to form a nematic phase, which can then form hydrogen bonds with the hard segment of SMPU40. On the other hand, as the DOBA content increases, the compatibility of SMPU40 with DOBA worsens, and hence, the crystallization rate of the hard segment of SMPU40 declines.

Liquid crystalline properties

The phase transition behaviors of the DOBA and SMPU40/DOBAm composites were further investigated via polarized optical microscopy (POM). To maintain consistency with the DSC results (for the second heating step), all the samples were heated to the same high temperature used for the DSC tests and then slowly cooled to room temperature. Typical POM textures of DOBA upon heating were recorded as shown in Fig. 8. The POM images show that DOBA formed a colorful crystalline texture below 80 °C (see Fig. 8a, b). When slowly heated to 115 °C, DOBA became soft, and its colorful texture turned into a smectic LC texture (Fig. 8c). Under this heating procedure, the samples exhibited a nematic LC texture at 136 °C (see Fig. 8d) [27]. Upon continuous heating, the LC texture began to disappear when the temperature reached approximately 145 °C (see

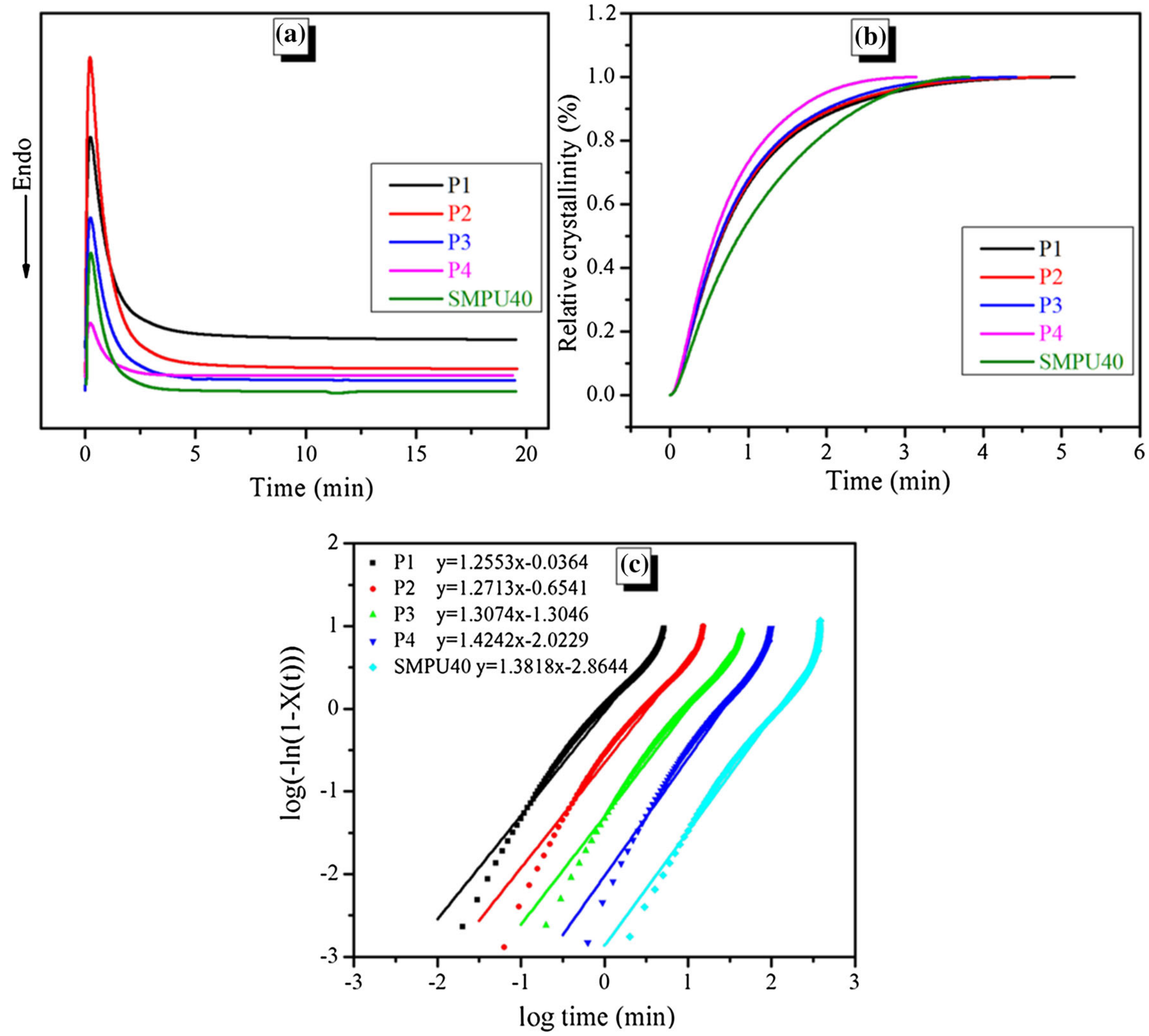

Fig. 7 Isothermal crystallization of the SMPU40/DOBAm composites. **a** Exothermic curves versus time. **b** Dependency of relative crystallinity versus time. **c** Plots of $\log\{-\ln[1-X(t)]\}$ versus $\log t$ and the fitting line at 137 °C.

Table 2 Isothermal crystallization kinetic parameters for SMPU40/DOBAm composites

Sample	n	$\ln K$	K	$t_{1/2}$
P1	1.2553	−0.0364	0.9642	0.7687
P2	1.2713	−0.6541	0.5199	1.2538
P3	1.3074	−1.3046	0.2713	2.0493
P4	1.4242	−2.0229	0.1323	3.1996

Fig. 8e). A corresponding exothermic peak appeared at this point on the DSC curve (see Fig. 4a).

POM images of P4 are shown in Fig. 9 as an example SMPU40/DOBAm composite. To prevent thermal decomposition, the POM detection temperature was below 200 °C. As shown in Fig. 9a, P4 formed a bright abundant crystalline texture at 40 °C due to the crystallization of the soft segment of SMPU40 mixed with the DOBA. When heated to 80 °C, as shown in Fig. 9b, P4 became darker. This phenomenon was due to the crystal melting of the soft segment of SMPU40, and the crystalline texture of the soft segment disappeared. When the temperature reached 96 °C, the image of P4 further darkened (seen Fig. 9c), indicating that the DOBA converted to a smectic phase, which was also detected in the DSC curve (see Fig. 4b). The POM image at 117 °C shows the nematic phase during the heating procedure, as a result of the DOBA mesogens. When the temperature reached 122 °C, the LC texture disappeared, and the field of vision became dark (Fig. 9e), indicating the isotropic state. The sample P4 tended to present another crystalline phase that

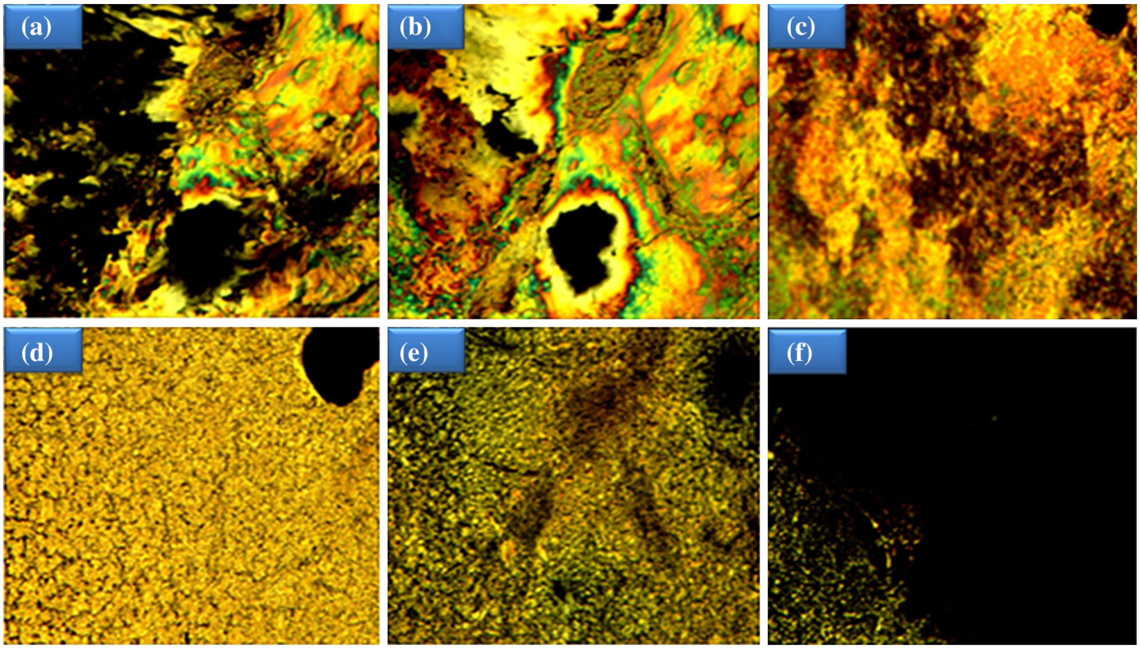

Fig. 8 Representative POM images of DOBA during the heating process: **a** 40 °C, **b** 80 °C, **c** 115 °C, **d** 136 °C, **e** 138 °C, and **f** 145 °C (×400 magnification).

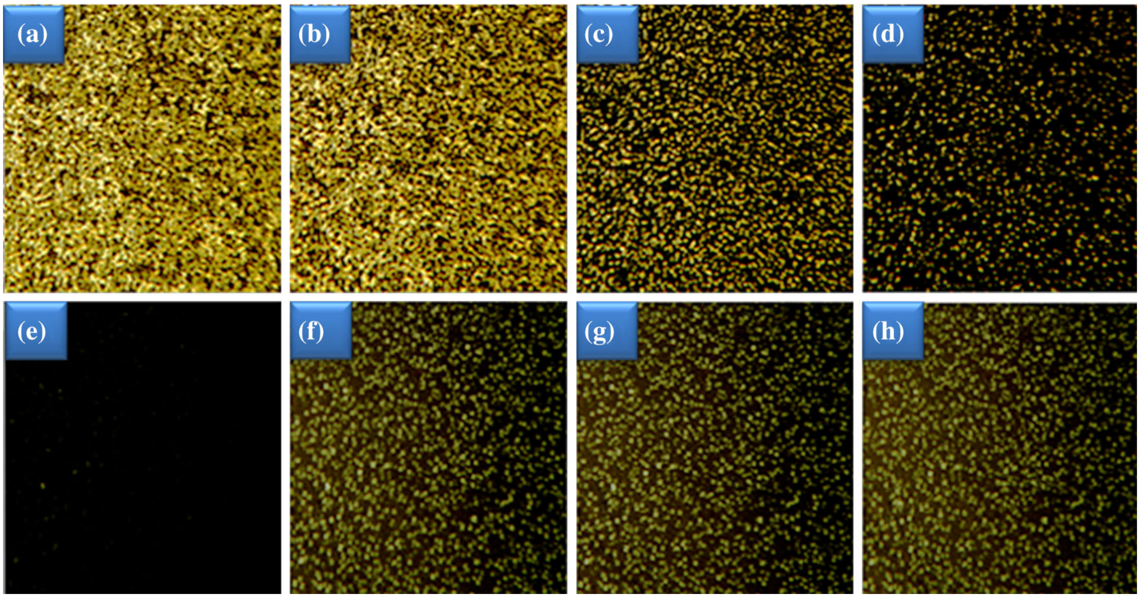

Fig. 9 Representative POM images of P4 during the heating process: **a** 40 °C, **b** 80 °C, **c** 96 °C, **d** 117 °C, **e** 122 °C, **f** 126 °C, **g** 150 °C, and **h** 195 °C (×400 magnification).

began at 126 °C. This crystalline texture should ascribe to the crystals of the hard segment of SMPU40, because this crystal phase is still maintained at 195 °C. We considered the following mechanism to explain this phenomenon: the crystallization capacity of the hard segment of SMPU40 was promoted after DOBA doping.

In addition, a comparison study of the POM textures for P1, P2, P3, and P4 at the same temperature (140 °C) are presented in Fig. 10. The POM images

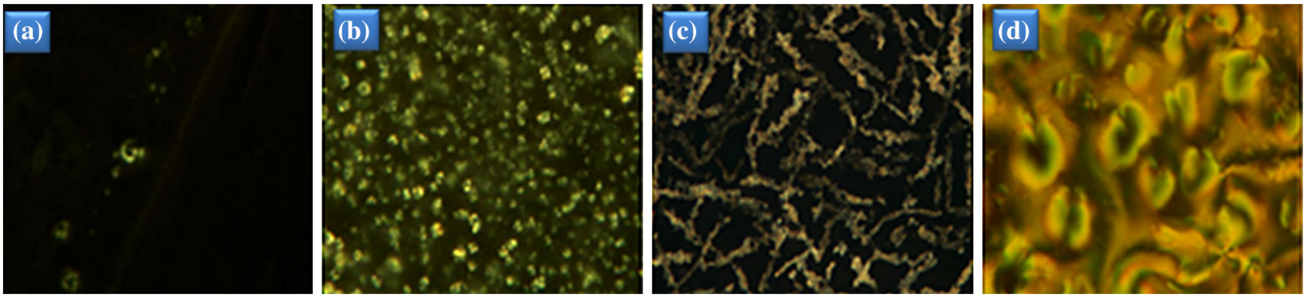

Fig. 10 POM images of **a** P1, **b** P2, **c** P3, and **d** P4 at 140 °C (×400 magnification).

demonstrated that in the composites with the low DOBA content, e.g., samples P1 and P2, the DOBA was completely distributed in the SMPU40 (Fig. 10a, b), and the DOBA formed fewer aggregates in the composites. However, as shown in Fig. 10c, P3 displayed an independent nematic phase. Moreover, as the DOBA content increased, the DOBA in the P4 formed continuous liquid crystalline phase. It was therefore further confirmed that some DOBA mesogens were free to be self-assembled, thus presenting the liquid crystalline phase. As shown in Fig. 10d, the POM image of P4 reveals a bright nematic phase throughout the entire view. Therefore, it is clear that the doped DOBA exhibited a nematic phase after melting of the crystal, because the polyurethane chains may prevent the formation of high-order DOBA aggregation. This observation is consistent with the DSC results presented above.

Shape memory properties

Recently, multishape-memory polymers have attracted significant attention and can be used to form complex polymer architectures [33]. In previous reports, we successfully developed a facile and versatile method to prepare LC-SMPCs with multi-SMEs [25, 26]. All SMPU-HOBA systems and SMPU-OOBA systems exhibited triple-SMEs, which could take on two temporary shapes in a single shape memory cycle. In this experiment, the triple-shape memory properties of the SMPU40/DOBAm composites were investigated using a DMA instrument according to the procedure described in our previous work. The rectangular samples were first elongated at 100 °C, and then fixed at low temperature, followed by recovery at 80 and 100 °C, for 40 min. The strain recovery process and its dependence on temperature change were recorded. Figure 11 presents the strain–time–temperature curves of samples P1, P2, P3, and P4, respectively. Figure 11 demonstrates that all the composites showed a two-step shape recovery. For instance, in the first step, P4 recovered 46.6 % of its strain at 80 °C, and the remaining 23 % strain was quickly recovered when the temperature was increased to 100 °C. Finally, more than 81 % of the total strain was recovered when the temperature maintained at 100 °C for approximately 20 min. The second step strain recovery temperature corresponded exactly to the melting temperature of the DOBA crystals (at 97 °C), as mentioned in DSC and POM test results. Moreover, the recovered strain in the second step tended to be much higher in the SMPU40/DOBAm composites with higher DOBA content. These results confirm that the second step strain recovery was associated with the melting transition of the DOBA crystals. Thus, the first step strain recovery was principally caused by the crystal melting transition of the soft segment of SMPU40. In addition, the SMPU40/DOBAm composite with the lower DOBA content exhibited a higher shape recovery ratio, and therefore, we considered that DOBA modifies SMPU40 as a type of plasticizer. Although the crystallizability of the hard segment of SMPU40 was enhanced, some of the DOBA molecules in the composites may destroy the entire network structure of SMPU40, resulting in permanent deformation. However, most of the SMPU40/DOBAm composites showed the typical triple-SMEs. Compared with the previous SMPU-HOBA and SMPU-OOBA systems, the entire shape recoveries of the SMPU40/DOBAm composites were improved due to the enhanced crystallizability of the hard segment.

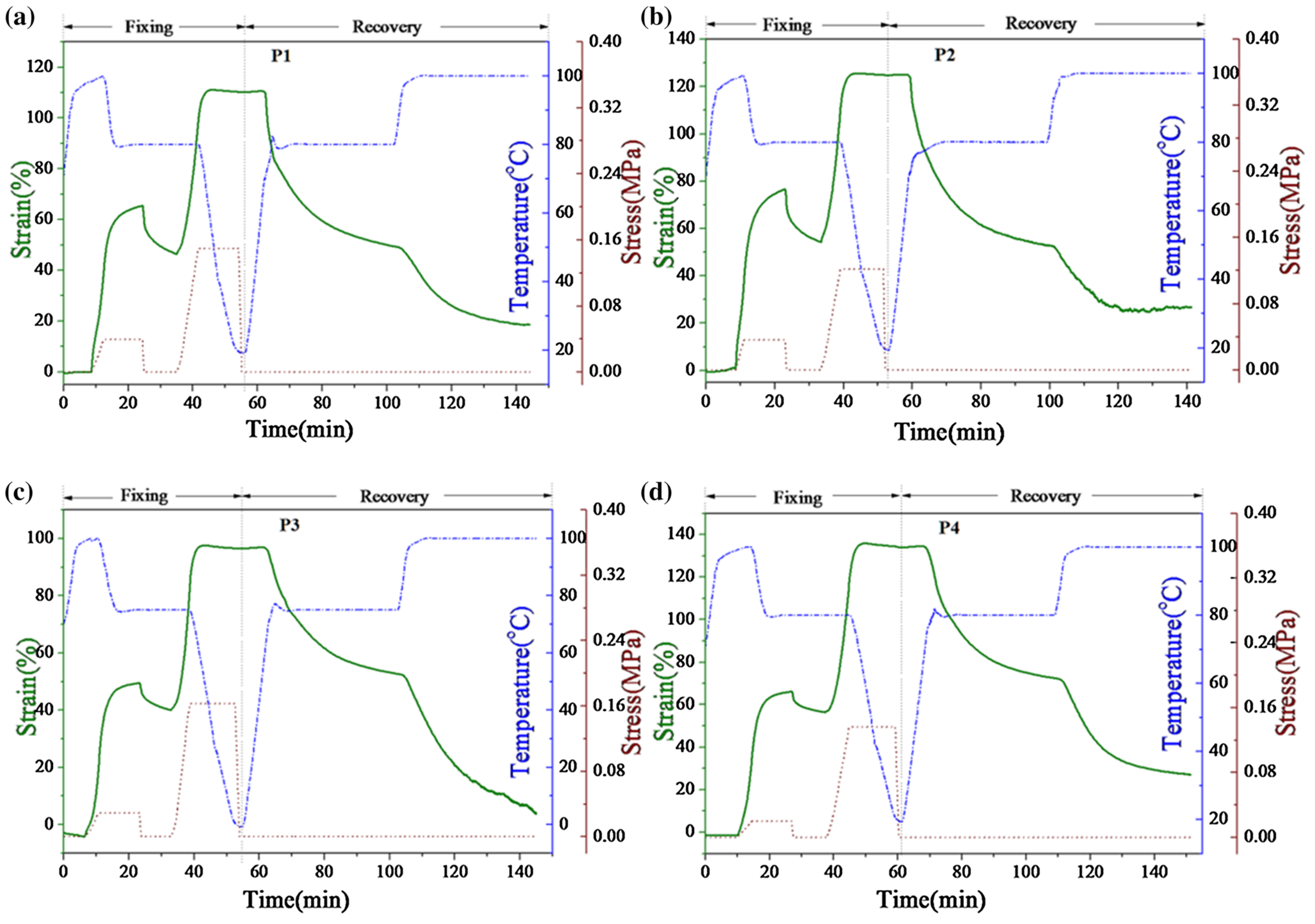

Fig. 11 Strain–time–temperature curves showing triple-shape memory effects for **a** P1, **b** P2, **c** P3, and **d** P4.

Conclusions

In this study, to elucidate the influence of LC filler on the structure and properties of LC-SMPU composites, PEG-based SMPU containing 40 wt% hard segments content was selected as a polymer matrix, and DOBA composed of both a smectic LC phase and a nematic LC phase was used as LC filler. Thus, a series of SMPU40/DOBAm composites were successfully prepared by adding various concentrations of DOBA to SMPU40. The structure, morphology, thermal properties, liquid crystalline properties, and shape memory properties were systematically investigated. The results demonstrate that DOBA was successfully incorporated into the polymer matrix of SMPU40 without interrupting the dimerization structure and while maintaining the basic structural LC properties of DOBA. The incorporated DOBA not only improves the crystallizability of the soft segment but also promotes the crystallizability of the hard segment. The isothermal crystallization kinetics revealed that the crystallization rate of the hard segment decreased as the DOBA content increased. The crystallization mechanism of the SMPU40/DOBAm composites nucleated in very similar manners. Overall, the SMPU40/DOBAm composites are composed of a DOBA phase and an SMPU40 phase, which further forms a soft phase–hard phase microphase separation structure. The incorporated DOBA includes polyurethane wrapped DOBA and a free DOBA aggregation phase. The composite tends to only maintain the nematic LC properties of DOBA due to the interruption of polyurethane chains. However, the SMPU40/DOBAm composites exhibit good triple-SMEs. The first step of strain recovery is associated with the melting transition of soft segment crystals of the polyurethane matrix, and the second step of strain recovery due to the melting transition of the DOBA crystals.

Acknowledgements

This work was supported by the National Natural Science Foundation of China (Grant Nos. 61425007, 61377090, and 61575128), the Natural Science Foundation of Guangdong (Grant No. 2014A030313559, 2016A030313050), the Special Research Foundation of Shenzhen Overseas High-level Talents for Innovation and Entrepreneurship (Grant No. KQCX20120807 153115869), the Nanshan District Key Lab for Biopolymers and Safety Evaluation (No. KC2014ZDZ J0001A), the Science and Technology Project of Shenzhen City (Grant No. JCYJ20140828163633993, ZDSYS201507141105130, CYZZ20150827160341635), and the project T201501 from Shenzhen Key Laboratory of Special Functional Materials.

References

[1] Meng H, Li G (2013) A review of stimuli-responsive shape memory polymer composites. Polymer 54:2199–2221

[2] Calvo CT, Santamaria EA (2015) Thermally-responsive biopolyurethanes from a biobased diisocyanate. Eur Polym J 70:173–185

[3] Leng J, Wu X, Liu Y (2009) Infrared light-active shape memory polymer filled with nanocarbon particles. J Appl Polym Sci 114:2455–2460

[4] Sun L, Huang WM (2010) Thermo/Moisture responsive shape-memory polymer for possible surgery/operation inside living cells in future. Mater Des 31:2684–2689

[5] Hu JL, Zhu Y, Huang HH, Lu J (2012) Recent advances in shape memory polymers: structure, mechanism, functionality, modeling and applications. Prog Polym Sci 37:1720–1763

[6] Ota S (1981) The heat shrinkage properties of polyethylene. Radiat Phys Chem 18:81–84

[7] Zhou YJ, Guan FL, Qian LF (2011) The application of shape memory polymer composite in space deployable truss structure. Adv Mater Res 287:2756–2759

[8] Khaldi A, Elliott JA, Smoukov SK (2014) Electro-mechanical actuator with muscle memory. J Mater Chem C 2:8029–8034

[9] Wang QH, Bai YK, Chen Y, Ju JP, Zheng F, Wang TM (2015) High performance shape memory polyimides based on π–π interactions. J Mater Chem A 3:352–359

[10] Haberl JM, Sanchez-Ferrer A, Mihut AM, Dietsch H, Hirt AM, Mezzenga R (2014) Light-controlled actuation, transduction, and modulation of magnetic strength in polymer nanocomposites. Adv Funct Mater 24:3179–3186

[11] Lee YM, Jin KS (1995) Preparation of pH/temperature responsive polymer membrane by plasma polymerization and its riboflavin permeation. Polymer 38:1227–1232

[12] Lin JR, Chen LW (1998) Study on shape-memory behavior of polyether-based polyurethanes. II. Influence of soft-segment molecular weight. J Appl Polym Sci 69:1575–1586

[13] Mo F, Zhou F, Chen S, Yang H, Ge Z, Chen S (2015) Development of shape memory polyurethane based on polyethylene glycol and liquefied 4,4′-diphenylmethane diisocyanate using a bulk method for biomedical applications. Polym Int 64:477–485

[14] Deka H, Karak N, Kalita RD, Buragohain AK (2010) Biocompatible hyperbranched polyurethane/multi-walled carbon nanotube composites as shape memory materials. Carbon 48:2013–2022

[15] Koerner H, Price G, Pearce NA, Alexander M, Vaia RA (2004) Remotely actuated polymer nanocomposites-stress-recovery of carbon-nanotube-filled thermalplastic elastomers. Nat Mater 3:115–120

[16] Kumar UN, Kratz K, Wagermaier W, Behl M, Lendlein A (2010) Non-contact actuation of triple-shape effect in multiphase polymer network nanocomposites in alternating magnetic field. J Mater Chem 20:3404–3415

[17] Weigel T, Mohr R, Lendlein A (2009) Investigation of parameters to achieve temperatures required to initiate the shape-memory effect of magnetic nanocomposites by inductive heating. Smart Mater Struct 18:1282–1294

[18] Lendlein A, Zotzmann J, Hofmann MBD (2010) Reversible triple-shape effect of polymer networks containing polypentadecalactone—and poly (ε-caprolactone)-Segments. Adv Mater 22:3424–3429

[19] Huang H, Geng J, He S, Li B, Ouyang C, Yin Y, Cao H, Wang L, Hai M, Wang G, Yang H (2007) Electrically induced and thermally erased properties of side-chain liquid crystalline polymer/liquid crystal/chiral dopant composites. Liq Cryst 34:949–954

[20] Mather PT, Burke KA (2010) Soft shape memory in main-chain liquid crystalline elastomers. J Mater Chem 20:3449–3457

[21] Tatsumi M, Teramoto Y, Nishio Y (2012) Polymer composites reinforced by locking-in a liquid-crystalline assembly of cellulose nanocrystallites. Biomacromolecules 13:1584–1591

[22] Finkelmann H, Happ M, Portugal M, Ringsdorf H (1978) Liquid crystalline polymers with biphenyl-moieties as mesogenic group. Makromol Chem 179:2541–2544

[23] Ahir SV, Tajbakhsh AR, Terentjev EM (2006) Self-assembled shape-memory fibers of triblock liquid-crystal polymers. Adv Funct Mater 16:556–560

[24] Chen S, Yuan H, Chen S, Yang H, Ge Z, Zhuo H, Liu J (2014) Development of supramolecular liquid-crystalline polyurethane complexes exhibiting triple-shape functionality using a one-step programming process. J Mater Chem A 2:10169–10181

[25] Chen S, Yuan H, Zhuo H, Chen S, Yang H, Ge Z, Liu J (2014) Development of liquid-crystalline shape-memory polyurethane composites based on polyurethane with a semi-crystalline reversible phase and hexadecyloxybenzoic acid for self-healing applications. J Mater Chem C 2:4203–4212

[26] Chen S, Mo F, Chen S, Ge Z, Yang H, Zuo J, Liu X, Zhuo H (2015) New insights into multi-shape memory behaviors and liquid crystalline properties of supramolecular polyurethane complexes based on pyridine containing polyurethane and 4-octyldecyloxy-benzoic acid. J Mater Chem A 3:19525–19538

[27] Prabu NPS, Mohan MLN (2013) Thermal analysis of hydrogen bonded benzoic acid liquid crystals. J Therm Anal Calorim 113:811–820

[28] Ambrozic G, Mavri J, Zigon M (2002) Liquid-crystalline complexes of polyurethane containing an isonicotinamide moiety with 4-dodecyloxybenzoic acid. Macromol Chem Phys 203:439–447

[29] Kato T, Fréchet JMJ (1995) Hydrogen bonding and the self-assembly of supramolecular liquid-crystalline materials. Macromol Symp 98:311–326

[30] Chen H, Liu Y, Gong T, Wang L, Zhao K, Zhou S (2013) Use of intermolecular hydrogen bonding to synthesize triple-shape memory supermolecular composites. Rsc Adv 3:7048–7056

[31] Huang J, Xu W (2010) Zwitterionic monomer graft copolymerization onto polyurethane surface through a PEG spacer. Appl Surf Sci 256:3921–3927

[32] Chen S, Mo F, Yang Y, Stadler FJ, Chen S, Yang H, Ge Z (2015) Development of zwitterionic polyurethanes with multi-shape memory effects and self-healing properties. J Mater Chem A 3:2924–2933

[33] Ware T, Hearon K, Lonnecker A, Wooley KL, Maitland DJ, Voit W (2012) Triple-shape memory polymers based on self-complementary hydrogen bonding. Macromolecules 45:1062–1069